



## Effects of 2-buthyne-1,4-diol additive on electrodeposited Ni films from a Watts-type bath

Takeshi Sakamoto<sup>a,b,\*</sup>, Kazuhisa Azumi<sup>a</sup>, Hiroto Tachikawa<sup>a</sup>, Kei Iokibe<sup>a</sup>, Masahiro Seo<sup>a</sup>, Nobuya Uchida<sup>c</sup>, Yasunaga Kagaya<sup>c</sup>

<sup>a</sup> Division of Materials Chemistry, Graduate School of Engineering, Hokkaido University, Sapporo 060-8628, Japan

<sup>b</sup> Technology Group, TDK Corporation, Saku 385-0009, Japan

<sup>c</sup> Technology Group, TDK Corporation, Ichikawa 272-8558, Japan

### ARTICLE INFO

#### Article history:

Received 11 May 2010

Received in revised form 11 July 2010

Accepted 11 July 2010

Available online 16 July 2010

#### Keywords:

Ni electrodeposition

2-Buthyne-1,4-diol

Preferred orientation

Morphology

Overpotential

### ABSTRACT

Structures of Ni films electrodeposited from a Watts-type bath containing 2-buthyne-1,4-diol (BD) were investigated using SEM, cross-sectional SIM, XRD measurement with a pole profiling technique and electrochemical methods for controlling properties of Ni electrodeposits. Preferred orientation of Ni electrodeposits was assigned to potential domains for electrodeposition. Preferred orientation in the higher potential region was (1 1 0) or (1 0 0), that in the middle potential region were (1 1 1) and (3 1 1), and that in the lower potential region was (1 0 0). The growing axis of Ni electrodeposits seems to agree with the speculation from Pangarov's model based on the two-dimensional nuclei theory in the lower overpotential region in which the dominant growing plane is fundamentally determined by crystallization overpotential related to supersaturation of adatom, although the growth axes of Ni deposits do not always agree with the preferred orientation. For example, preferred orientation of (1 1 0) was assigned to growing (1 1 1) plane which tilts at 55° to the substrate. Adsorption of BD affects the structure and morphology of electrodeposits via an inhibitory effect related to its surface coverage depending on surface orientation, growth rate and BD concentration in the plating bath.

© 2010 Elsevier Ltd. All rights reserved.

### 1. Introduction

Ni electrodeposition has been widely used for corrosion protection and for attractive appearance of iron, steel, copper and many other alloys. Ni electrodeposition has also recently been used for the fabrication of electronic devices. For example, Ni-based corrosion protective plating layers formed on strong magnets composed of rare earth elements are used for actuators of data storage hard disk drives and hybrid automobiles. Ni electrodeposition has also been applied to connectors and printed circuit boards (PCB) for assurance of reliable connection between electric/electronic components.

Crystallographic structure and its orientation of Ni electrodeposits are related to various properties of plating films such as corrosion resistance, hardness, magnetic properties, and contact resistance [1]. For example, anodic dissolution rate of different Ni grains is in the order of (1 1 0) > (1 0 0) > (1 1 1) [2]. Corrosion protective duplex Ni plating layer consists of a top layer composed of micro-grain crystals containing sulfur and an under layer composed of columnar crystals, and the former acts as sacrificial anode in corrosion reaction to protect under layer and substrate

[3]. Thickness of air formed oxide film on Ni grain is in the order of (1 1 0) > (1 0 0) > (1 1 1) [4], and thus low resistive electric contact is obtained for Ni deposits with (1 1 1) or (1 0 0) orientation [5,6]. Organic additives adsorb on Ni surface with their unsaturated molecular bonds [7] to block the sites for Ni deposition and alternate deposition rate depending on their crystal orientation [8]. For example, 2-buthyne-1,4-diol (BD) has been used as one of major organic additives for controlling structure of Ni electrodeposits due to its triple bond.

Structure of Ni electrodeposits has been intensively investigated by many researchers. In 1916, Watts developed a high-speed Ni electrodeposition solution called a Watts-type bath [9], which has since been used worldwide. Schlöttor [10] developed bright Ni electrodeposition from a sulfate solution containing Ni ions and organic additives. Kardos et al. introduced BD as an additive to obtain a highly smooth and sulfur-free Ni electrodeposited film [11]. In the 1960s, Ni-based double layer coating, in which a bright Ni film containing sulfur was deposited on a sulfur-free Ni electrodeposited film, was developed [12]. Fischer categorized the structures of an electrodeposited film into six types as [13–17] FI (field-oriented isolated crystals) type, BR (basis-oriented reproduction) type, Z (twinning intermediate) type, FT (field-oriented texture) type, UD (unoriented dispersion) type and RL (rhythmic-lamellar) type. For example, it was reported that a sulfur-free Ni electrodeposited film

\* Corresponding author. Tel.: +81 67661111; fax: +81 67684515.

E-mail address: [faraday@cyber.email.ne.jp](mailto:faraday@cyber.email.ne.jp) (T. Sakamoto).

was composed of columnar crystals assigned to FT-type [3] and that a bright Ni electrodeposited film containing sulfur was composed of fine crystals assigned to UD-type. Winand summarized Fischer's classification in a Winand's diagram [18–20]. FT-type electrodeposits are observed in the fairly strong inhibition condition due to adsorption of additives and are composed of elongated crystals or columnar crystals almost perpendicular to the substrate. UD-type electrodeposits are observed in the condition of very strong inhibition and are composed of very fine crystalline particles randomly oriented.

Many researchers have reported the relationship between preferred orientation of Ni electrodeposits and inhibition effect. Reddy et al. [21–23] proposed that the preferred orientation of Ni electrodeposits tends to be (111) in free growth conditions and changes sequentially to (100), (110) or (211) with increase in hydrogen adsorption. Amblard et al. [24] proposed that preferred orientation of (211) and (111) for Ni electrodeposits was provided by the inhibition effect of colloidal Ni(OH)<sub>2</sub> adsorption, and preferred orientation of (110) and (210) for Ni electrodeposits was provided by the inhibition effect of hydrogen adsorption. This idea is consistent with the finding by Motoyama et al. [25] that the equilibrium line between (110) and (100) orientations of Ni in the Pourbaix diagram was almost parallel to the equilibrium line of hydrogen gas evolution. Addition of BD to a Watts-type bath also affects the orientation of Ni electrodeposits. Macheras et al. [26] investigated the preferred orientation of Ni films electrodeposited from a Watts-type bath containing several kinds of organic additives. They showed that addition of acetylenic compounds to a Watts-type bath greatly inhibits crystal growth.

These previous investigations have clearly indicated that the structure of Ni electrodeposits is affected by many factors of electrodeposition conditions. However, the role and effect of these additives have not yet been elucidated. Watanabe [27] reported that various physical properties of electrodeposits were closely connected to their microstructures such as size and orientation of microcrystalline, surface morphology, metallurgical structures of substrate, and so on. In this work, therefore, structures of Ni films electrodeposited from a Watts-type bath containing BD were investigated as a function of electrodeposition conditions.

## 2. Experimental

A polycrystalline copper sheet of 10 mm × 30 mm × 0.5 mm in size was used for plating of the substrate. The sheet was mechanically polished and dipped in solution containing 0.2 mol cm<sup>-3</sup> NaOH, 0.15 mol dm<sup>-3</sup> Na<sub>2</sub>CO<sub>3</sub> and 0.2 mol dm<sup>-3</sup> Na<sub>4</sub>SiO<sub>4</sub> at 323 K for 300 s for cleaning the substrate surface before electrodeposition. A Watts-type bath containing 0.0, 0.2 or 1.0 mmol dm<sup>-3</sup> 2-buthyne-1,4-diol (BD) was prepared from analytical-grade chemicals as shown in Table 1. The pH of the bath was adjusted to 4.0 by adding sodium hydroxide, and the temperature of the bath was maintained at 323 K during electroplating. A series of combination of BD concentration and current density shown in Table 2 was used to obtain Ni films of ca. 10 μm in thickness in a stagnant condition. Many previous laboratory studies have been performed in a stirring con-

**Table 1**

Composition of the Watts-type bath and the electrodeposition conditions for Ni electroplating.

|  |  |
|--|--|
| Ni sulfate hexahydrate (NiSO <sub>4</sub> ·6H <sub>2</sub> O)  | 1.0 mol dm <sup>-3</sup>               |
| Ni chloride hexahydrate (NiCl <sub>2</sub> ·6H <sub>2</sub> O) | 0.2 mol dm <sup>-3</sup>               |
| Boric acid (H <sub>3</sub> BO <sub>3</sub> )                   | 0.7 mol dm <sup>-3</sup>               |
| 2-Buthyne-1,4-diol (HOCH <sub>2</sub> CCCH <sub>2</sub> OH)    | 0.0, 0.2, or 1.0 mmol dm <sup>-3</sup> |
| pH   | Adjusted to 4.0 by adding NaOH         |
| Temperature  | 323 K                                  |
| Current density  | 30, 100 or 300 A m <sup>-2</sup>       |

**Table 2**

Electrodeposition conditions for different samples.

| Sample | 2-Buthyne-1,4-diol (mmol dm <sup>-3</sup> ) | Current density (A m <sup>-2</sup> ) |
|--------|---|--------------------------------------|
| A-1    | 0.0   | 30                                   |
| A-2    | 0.0   | 100                                  |
| A-3    | 0.0   | 300                                  |
| B-1    | 0.2   | 30                                   |
| B-2    | 0.2   | 100                                  |
| B-3    | 0.2   | 300                                  |
| C-1    | 1.0   | 30                                   |
| C-2    | 1.0   | 100                                  |
| C-3    | 1.0   | 300                                  |

dition, while electrodeposition in practical production lines is done in a stagnant or mild stirring condition. To characterize the electrochemical properties of the plating system, polarization curves of a Cu working electrode of 0.2 cm<sup>2</sup> in area was measured in the plating bath deaerated with nitrogen gas bubbling using an electrochemical measurement system (Hokuto Denko Co. model HZ-5000), an Ag/AgCl/Sat. KCl reference electrode, and a platinum counter electrode. Electrode potential was swept from the immersion potential in a less-noble potential with a sweep rate of 2 mV s<sup>-1</sup>. Electrode potential presented in this paper refers to the standard hydrogen electrode (SHE) potential.

X-ray diffraction (XRD; PANalytical Co. model MPD) spectra were measured using Cu Kα radiation. Diffractograms were recorded in a range from 20 to 160° of 2θ with 0.02° step per 1 s. Pole figure and elevation profile was also obtained using X-ray diffraction equipment (XRD; Rigakudenki Co. model ATX-G). Surface morphology of Ni electrodeposits was observed using a scanning electron microscope (SEM; Hitachi Ltd., model S-800). For cross-sectional observation of electrodeposits, the specimen was etched using a focused ion beam (FIB, Hitachi Ltd., model FB-2100) with Ga ions to make a trench with angles of 90° to the surface and the etched surface, i.e., cross-section, was imaged with an observation angle of 45° (SIM image). The resultant cross-sectional image was thus compressed by 1/√2 in the vertical axes.

## 3. Results and discussion

### 3.1. Relationship between preferred orientation and polarization condition

Crystallographic orientation of Ni films electrodeposited from a Watts-type bath measured using XRD are summarized in Fig. 1 as a function of BD concentration and current density. Preferred orientations were (220) for samples A-1 and A-2, (200) for A-2 and B-1, (111) for B-2, C-1 and C-2, and (200) and (111) for A-3, B-3 and C-3. For further analysis of crystallographic orientation, intensity of the XRD peak of each orientation shown in Fig. 1 was normalized using the following equation:

$$M(hkl) = \frac{I(hkl)}{I_{\text{ICDD}}(hkl)}, \quad (1)$$

where  $M$  is the normalized intensity,  $I$  is the measured intensity of the XRD peak at a specific orientation ( $hkl$ ), and  $I_{\text{ICDD}}$  is the XRD intensity of an ICDD PDF2 database. In Fig. 2,  $M$  is plotted against deposition current density to compare the relative intensities for the orientations, and the following tendencies were found: (1) preferred orientations changed with BD concentration at a low current density, (2)  $M(200)$  drastically increased with current density, and (3)  $M$  of some orientations tended to increase with current density. However, the relationship between orientation and deposition condition is not so clear in these plots.

Many researchers have proposed the relationship between preferred orientations of electrodeposits and overpotential for

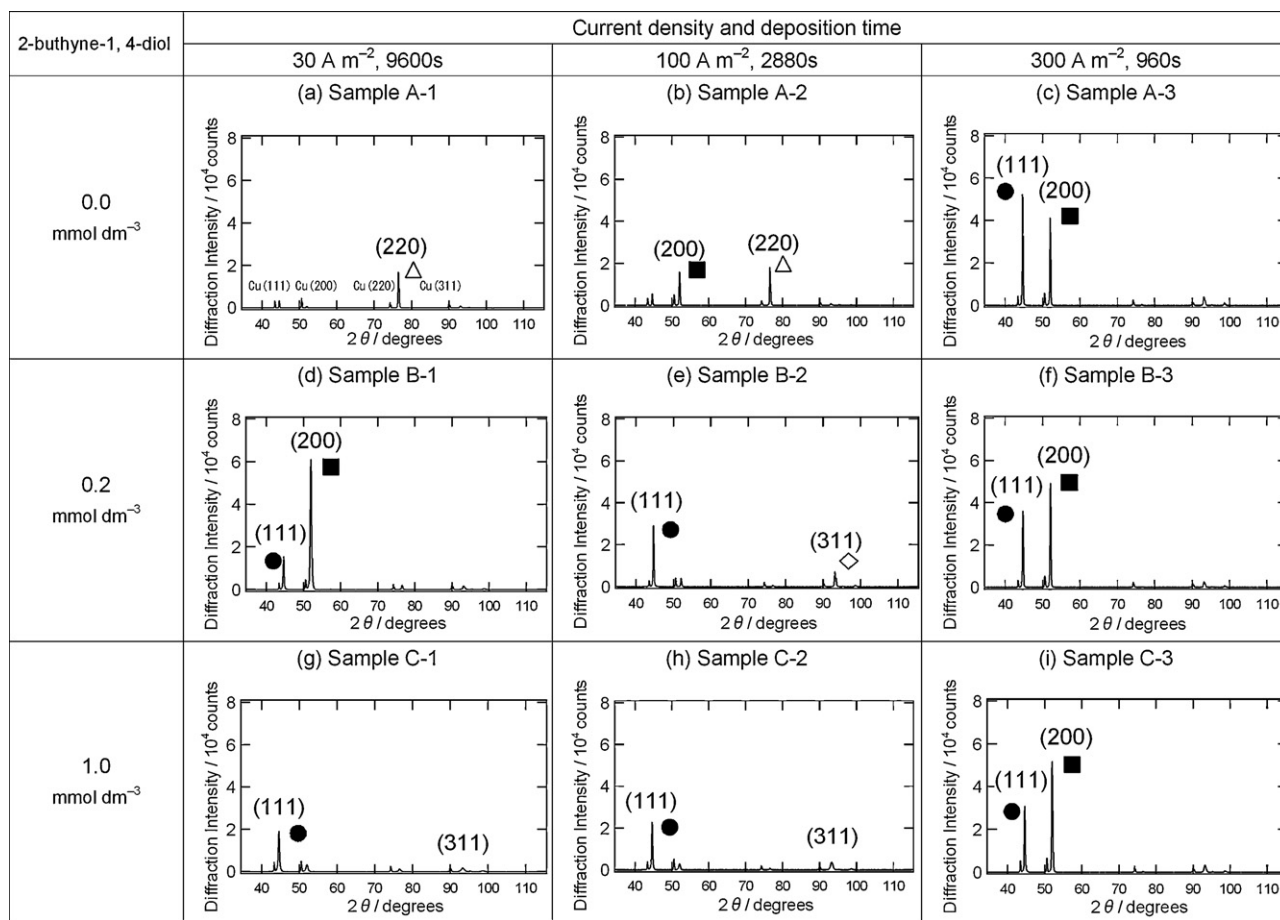


**Fig. 1.** XRD spectra of Ni films electrodeposited from a Watts-type bath containing  $0.0 \text{ mmol dm}^{-3}$  (a–c),  $0.2 \text{ mmol dm}^{-3}$  (d–f) or  $1.0 \text{ mmol dm}^{-3}$  (g–i) 2-buthyne-1,4-diol at current density of 30, 100 or  $300 \text{ A m}^{-2}$ . Preferred orientation of Ni crystalline is assigned as follows: triangle to (220), box to (200), circle to (111), and lozenge to (311).

electrodeposition [16,17,32,28–30]. In Fig. 3, cathodic polarization curves of the Ni electrode measured in a Watts-type bath are shown as a function of BD concentration. This plot clearly shows that deposition potential at the same current density shifts in a less-noble direction with increase in BD concentration. The polarization curves can be divided into three regions, i.e., Tafel region at lower overpotential, diffusion control region at higher overpotential, and transition region between them. The dashed straight lines show the Tafel relationship of three  $i$ - $E$  curves expressed by the following equations:

$$\text{Line 1, } 0.0 \text{ MBD: } \eta = 0.319 - 0.103 \log |i|, \quad (2)$$

$$\text{Line 2, } 0.2 \text{ MBD: } \eta = 0.450 - 0.232 \log |i|, \quad (3)$$

$$\text{Line 3, } 1.0 \text{ MBD: } \eta = 0.493 - 0.238 \log |i|. \quad (4)$$

Tafel slopes of lines 2 and 3 are almost identical and smaller than that of line 1, indicating that inhibition strengths of lines 2 and 3 due to BD are almost the same in the Tafel region. Transition from the Tafel region to the diffusion control region probably involves competition between formation of a fresh surface of Ni deposits and adsorption of BD onto this surface, and the rate of the latter depend on BD concentration. In the diffusion control region, BD does not affect Ni deposition anymore because the deposition rate is considerably faster than the adsorption rate of BD.

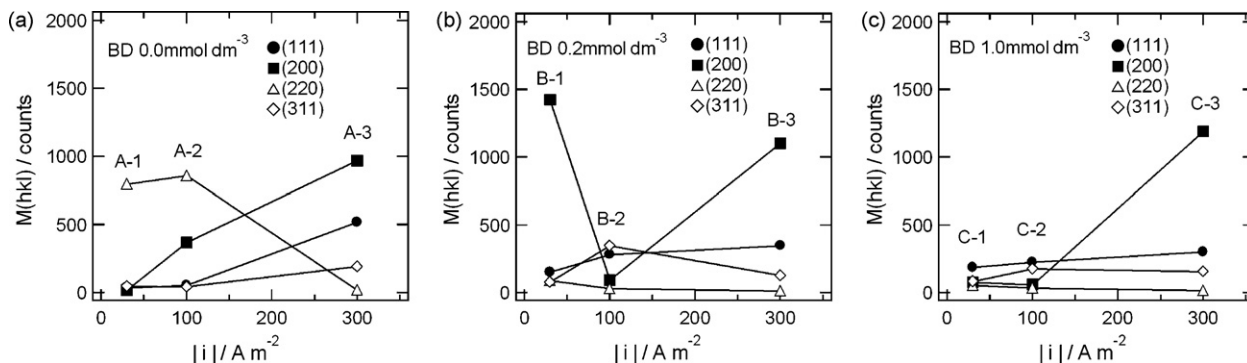


**Fig. 2.** Normalized XRD peak intensity,  $M(hkl)$ , obtained from data shown in Fig. 1 using Eq. (1) as a function of deposition current density at 30, 100 or  $300 \text{ A m}^{-2}$  and 2-buthyne-1,4-diol concentration at  $0.0 \text{ mmol dm}^{-3}$  (a),  $0.2 \text{ mmol dm}^{-3}$  (b) or  $1.0 \text{ mmol dm}^{-3}$  (c). Preferred orientation of Ni crystalline is assigned as follows: triangle to (220), box to (200), circle to (111), and lozenge to (311).

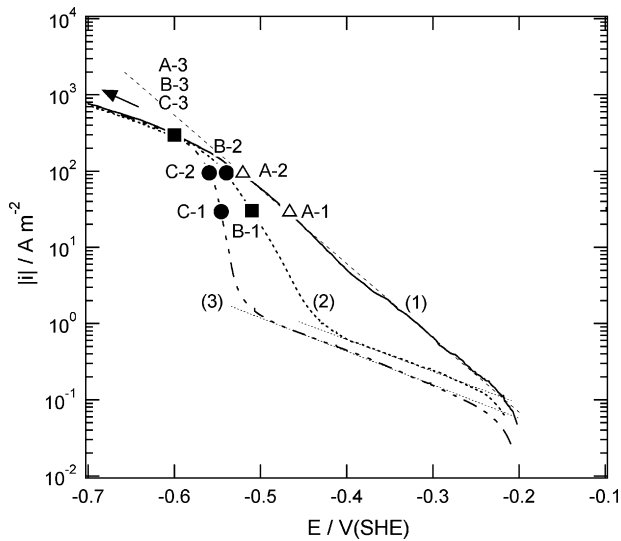


**Fig. 3.** Cathodic polarization curves of during Ni electrodeposition in a Watts-type bath containing 2-buthyne-1,4-diol at concentrations of (1) 0.0 mmol dm<sup>-3</sup>, (2) 0.2 mmol dm<sup>-3</sup>, and (3) 1.0 mmol dm<sup>-3</sup>. Symbols indicate preferred orientation of Ni electrodeposits obtained in Fig. 1 as triangle to (220), box to (200), circle to (111), and lozenge to (311).

The deposition potentials,  $E_d$ , which are the estimated values of  $E$  at each deposition current density,  $i$ , on three cathodic polarization  $i$ - $E$  curves shown in Fig. 3 as described by the symbols. A plot of  $M(hkl)$  against  $E_d$  shown in Fig. 4(a) clearly reveals the three domains. Fig. 4(b) is fractional expression of relative intensities of  $M(hkl)$  against  $E_d$ . Preferred orientations for each specimen is determined as dominant orientation higher than 50% of  $M(hkl)$ . Preferred orientations of samples A-1, A-2 and B-1 in the potential region higher than  $-0.53$  V (domain 1) are (220) or (200). Preferred orientations of samples B-2, C-1 and C-2 in the potential region from  $-0.54$  to  $-0.56$  V (domain 2) are (111) and (311). Preferred orientations of samples A-3, B-3 and C-3 in the potential region lower than  $-0.59$  V (domain 3) are (200).

### 3.2. Consideration of overpotential using the two-dimensional nuclei theory

In order to interpret the relationship between crystallographic orientation and overpotential of electrodeposition, we considered Fischer's model [13,16] and Pangarov's model based on two-dimensional nuclei theory [28–30]. Fischer considered components of total overpotential for electrodeposition,  $\eta$ , as the following relationship [13,16]:

$$\eta = \eta_t + \eta_d + \eta_r + \eta_\Omega + \eta_k, \quad (5)$$

where  $\eta_t$  is the charge transfer overpotential,  $\eta_d$  is the diffusion overpotential,  $\eta_r$  is the reaction overpotential,  $\eta_\Omega$  is the ohmic potential drop and  $\eta_k$  is the crystallization overpotential. Pangarov derived the work,  $W_{hkl}$ , required to form a two-dimensional nucleus of the  $(hkl)$  plane [28–30] as

$$W_{hkl} = \frac{B_{hkl}}{\frac{zF}{N}(\varphi - \varphi^*) - A_{hkl}}, \quad (6)$$

where  $z$  is the valency of ions,  $F$  is the Faraday constant,  $N$  is the Avogadro number,  $\varphi$  is an electrode potential at a given current density for electrodeposition,  $\varphi^*$  is an equilibrium potential for electrodeposition, and  $A_{hkl}$  and  $B_{hkl}$  are values related to the work for breaking a bond of some atom with its neighbor atoms at the  $(hkl)$  plane and its separation from the substrate. According to this equation,  $W_{hkl}$  depends on crystallization overpotential,  $\varphi - \varphi^*$ .

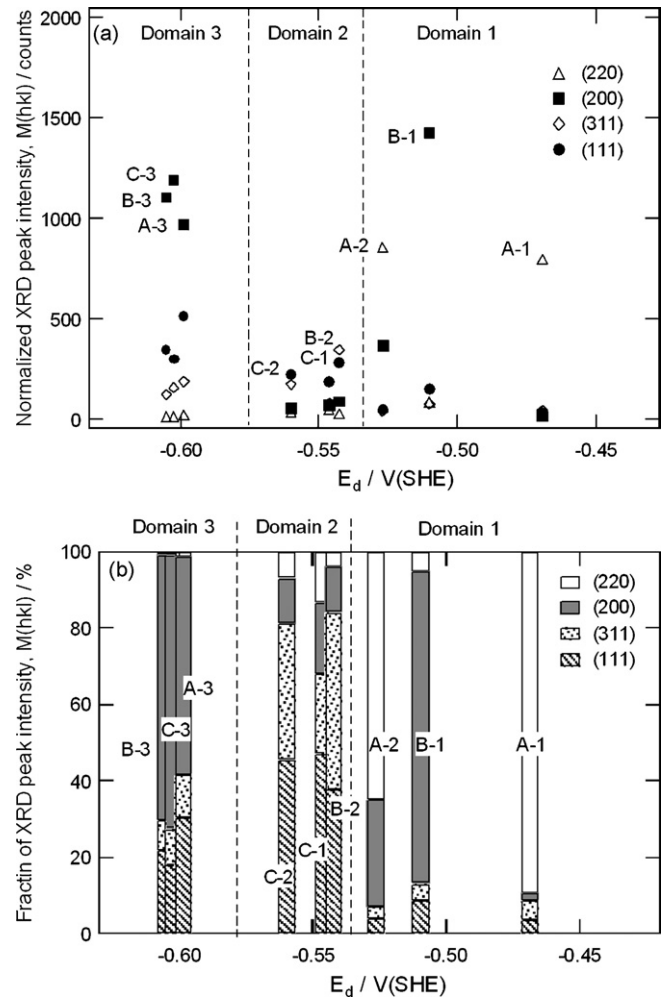


**Fig. 4.** (a) Relationship between normalized XRD peak intensity,  $M(hkl)$ , of Ni electrodeposited films and deposition potential,  $E_d$ . Preferred orientation of Ni crystal is assigned as follows: triangle to (220), box to (200), circle to (111), and lozenge to (311). (b) Relationship between the fraction of  $M(hkl)$  and  $E_d$ .

Pangarov evaluated  $W_{hkl}$  as a function of supersaturation,  $\sigma$ , for each lattice plane [28–30]. Supersaturation was considered as a driving force of crystallization and could be calculated from activity of adsorbed metal ions ( $M^{z+}$ ) under an equilibrium condition,  $a_{ad}^0$ , and that of cathodic polarization condition,  $a_{ad}$ , using the following equation [31,32]:

$$\sigma = \frac{a_{ad} - a_{ad}^0}{a_{ad}^0} = \frac{a_{ad}}{a_{ad}^0} - 1. \quad (7)$$

Nernst equations under these two conditions are defined as

$$\varphi^* = \varphi_0 + \frac{RT}{zF} \ln \frac{[M^{z+}]}{a_{ad}^0}, \quad (8)$$

$$\varphi = \varphi_0 + \frac{RT}{zF} \ln \frac{[M^{z+}]}{a_{ad}}, \quad (9)$$

where  $\varphi_0$  is the standard electrode potential,  $R$  is the gas constant, and  $T$  is the temperature. The crystallization overpotential in Eq. (5),  $\eta_k$ , is equal to  $\varphi - \varphi^*$  [31] and is described using Eqs. (8) and (9) as

$$\eta_k = \varphi - \varphi^* = \frac{RT}{zF} \ln \frac{a_{ad}^0}{a_{ad}} = -\frac{RT}{zF} \ln(\sigma + 1). \quad (10)$$

Pangarov predicted the preferred orientation for thick deposits of fcc metals such as Ag and Cu to be [111] at  $\sigma \leq 5.2$  in the low

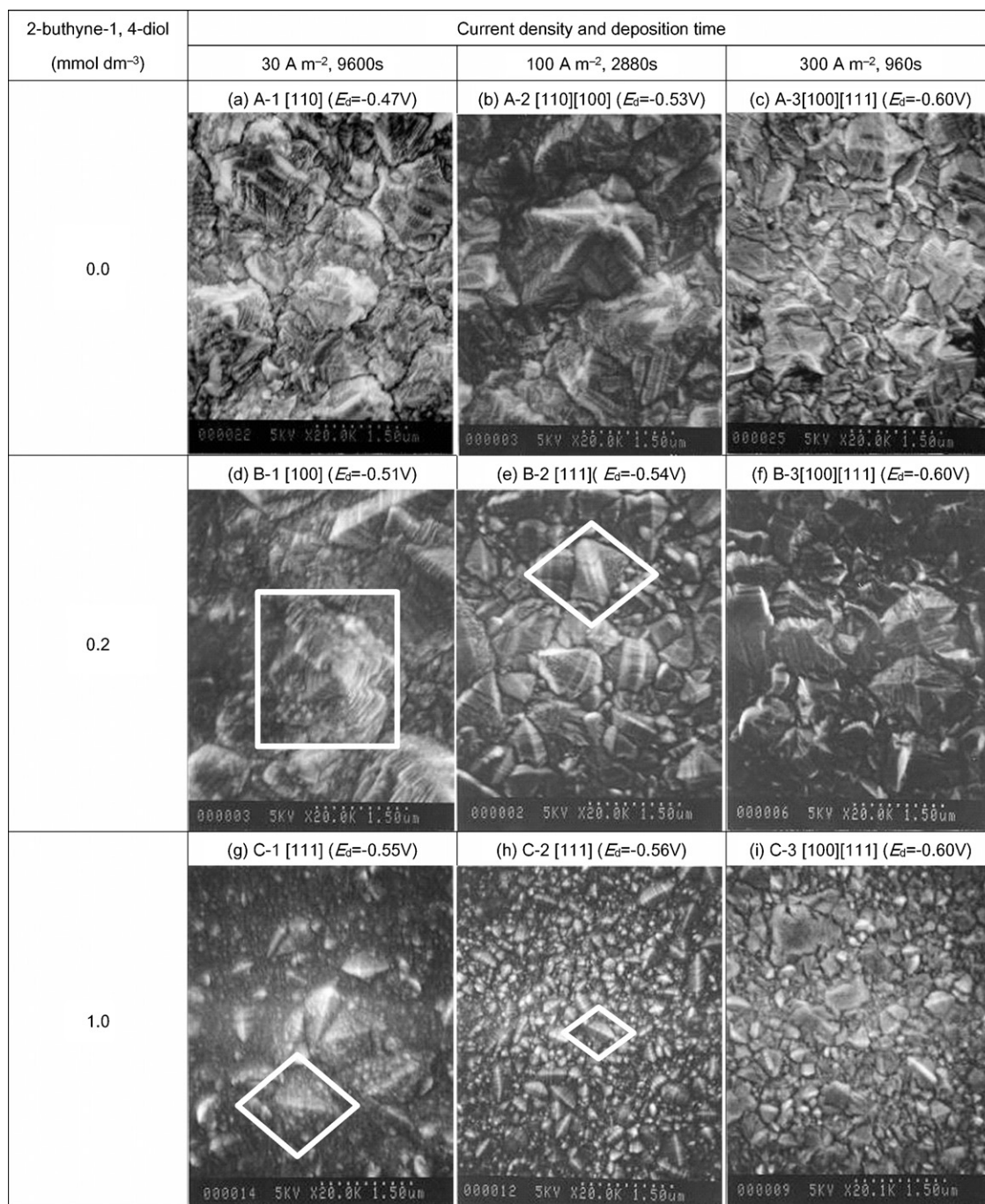


**Fig. 5.** SEM images of Ni films electrodeposited from a Watts-type bath containing 0.0, 0.2 or 1.0 mmol dm<sup>-3</sup> 2-buthyne-1,4-diol at current density of 30, 100 or 300 A m<sup>-2</sup>. The preferred orientation was obtained from XRD spectra shown in Fig. 1. The deposition potential,  $E_d$ , vs. SHE shown in parenthesis was estimated from cathodic polarization curves shown in Fig. 3.

overpotential region, [1 0 0] at  $5.2 < \sigma < 5.7$  in the intermediate overpotential region, and [1 1 0], [1 1 3] and [2 1 0] at  $\sigma \geq 5.7$  in the high overpotential region. This prediction was in good agreement with experimental results of electrodeposition of Ag and Cu and was also successfully applied to other metals with different crystalline types [30]. The values of  $\eta_k$  were calculated to be  $-0.025$  V at  $\sigma = 5.2$  and  $-0.026$  V at  $\sigma = 5.7$  using Eq. (10) with the conditions of  $T = 323$  K and  $z = 2$ . From the correspondence between  $\sigma$ ,  $\eta_k$  and preferred orientation described above, the preferred orientations of the fcc lattice form are predicted to be [1 1 1] at  $\eta_k \geq -0.025$  V, [1 0 0] at  $-0.026 < \eta_k < -0.025$  V, and [1 1 0] at  $\eta_k \leq -0.026$  V.

To verify the applicability of Pangarov's model to the present experimental results, the relationship between preferred orientation and electrode potential shown in Fig. 4(a) was examined. In domain 2, preferred orientation of samples B-2, C-1 and C-2 was [1 1 1] and thus  $\eta_k$  was expected to be  $\eta_k \geq -0.025$  V. In domain 3, preferred orientation for samples A-3, B-3 and C-3 was [1 0 0] and thus  $\eta_k$  was expected to be  $-0.026$  V  $< \eta_k < -0.025$  V. On the other hand, measured overpotential  $\eta$ , i.e., the potential difference between the deposition potential and the equilibrium potential of  $-0.20$  V (SHE) shown in Fig. 3, was  $-0.46$  to  $-0.53$  V in domain 1,  $-0.54$  to  $-0.56$  V in domain 2, and ca.  $-0.59$  V in domain 3. These

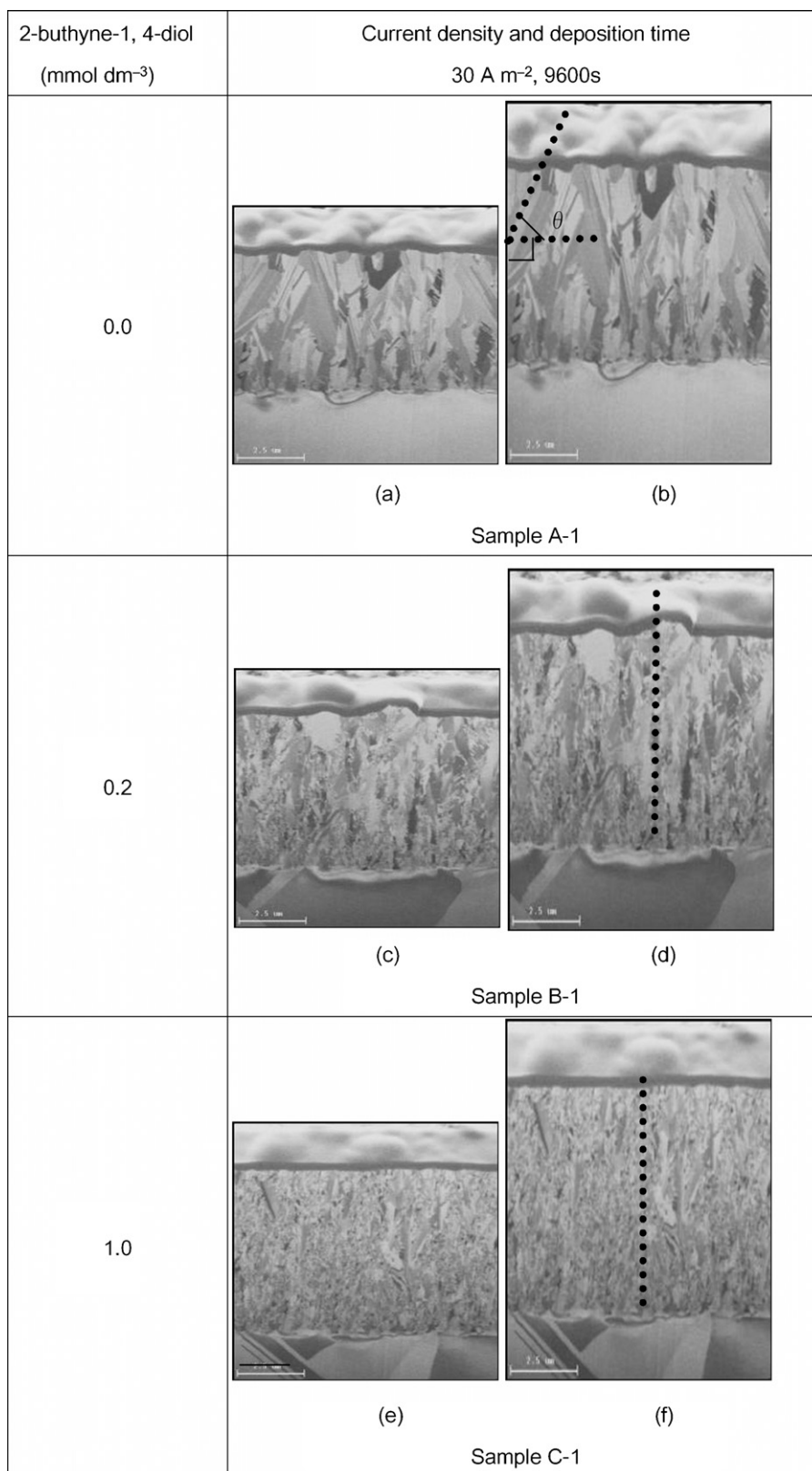


**Fig. 6.** Cross-sectional SIM images of Ni plating films deposited from a Watts-type bath containing 0.0 mmol dm<sup>-3</sup> (a and b), 0.2 mmol dm<sup>-3</sup> (c and d) and 1.0 mmol dm<sup>-3</sup> (e and f) of 2-buthyne-1,4-diol at current density of 30 A m<sup>-2</sup>. (a, c, e) are original images. (b, d, f) are corrected images obtained by expanding the vertical scale by  $\sqrt{2}$  (see text).

values of  $\eta$  were considerably larger than that of  $\eta_k$ , because  $\eta_k$  is a part of  $\eta$  as defined by Eq. (5). Although the contribution of  $\eta_k$  to  $\eta$  is considerably small, it may be possible to assign domain 2 where the preferred orientation is [1 1 1] to  $\eta_k \geq -0.025$  V and domain 3 where

the preferred orientation is [1 0 0] to  $-0.026$  V  $< \eta_k < -0.025$  V. In these assignments, however, domain 1 cannot be assigned to  $\eta_k$ . The reason for this discordance is discussed in the next subsection.

### 3.3. Morphology of Ni deposits

To investigate the reason for the inconsistency of preferred orientation of Ni electrodeposits obtained in the present experiments from that of Pangarov's prediction in domain 1, surface and cross-sectional morphologies of electrodeposits were observed using SEM and SIM. As shown in SEM images in Fig. 5, surface morphology changed depending on electrode potential and BD concentration. In these images, two typical structures can be recognized. One is spiral-type deposits found in the films deposited at  $-0.51$  V as indicated by a box in Fig. 5(d). The other is lozenge-type deposits indicated by diamond frames in Fig. 5(e) (g) and (h), and they were found on the films deposited at  $-0.54$  to  $-0.56$  V. The size of the lozenge structures decreased with increases in BD concentration and current density.

Fig. 6 shows cross-sectional SIM images of samples A-1, B-1 and C-1 electrodeposited at  $30 \text{ A m}^{-2}$ . The images on the left are original SIM images and the images on the right were obtained by multiplying the vertical scale of the left image by  $\sqrt{2}$  to reproduce the actual dimension of the cross-section because the observation angle was  $45^\circ$  to the cross-section. It seems that the incipient Ni electrodeposits are influenced from substrate, but crystal size gradually departs from the incipient electrodeposits, and finally the Ni electrodeposits have a crystal size the deposition conditions without substrate influence, as shown in Fig. 6. The substrate material is not as a critical factor for structure or preferred orientation of electrodeposits except for initial stage. This phenomenon was found by Finch and Williams [33] who summarized that the effect of substrate on crystal size and orientation gradually disappeared within  $3 \mu\text{m}$  from the interface, and the crystal size and orientation could be characterized by the electrodeposition condition.

In these images, grain size of Ni electrodeposits becomes small with increase in BD concentration. Sample A-1 is composed of thick columns inclined to the growth direction and the maximum incline angle is ca.  $58^\circ$  against the substrate plane. On the other hand, samples B-1 and C-1 are composed of narrow columns oriented perpendicularly to the substrate plane. In all samples, grain size is small at the interface between the film and substrate and increases with film growth.

Sample B-1 shows a spiral structures in the SEM image shown in Fig. 5(d) and strong (2 0 0) and weak (1 1 1) peaks in XRD spectra shown in Fig. 1(d). A cross-sectional SIM image of sample B-1 (Fig. 6(d)) indicates that the electrodeposits are composed of small crystals and large spiral crystals among them. The formation mechanism of such spiral structures in electrodeposits has been investigated by many researchers [13–20,32,34–36]. Generally, the crystal growth process involves surface diffusion of adatoms from terraces to steps and settlement at kinks [37] (TSK model). If a screw dislocation exists on the surface of the (1 0 0) plane, the spiral crystal grows in a direction normal to the surface, while the actual growth plane is (1 1 1) which orientation declines to the surface of the (1 0 0) plane as schematically shown in the top image of Fig. 8(b).

[1 1 0] orientation in sample A-1 can be explained as follows. The cross-sectional SIM image in Fig. 6(b) shows that the crystalline column inclines between  $58^\circ$  and  $90^\circ$  against the surface plane. Since the apparent incline angle of columns in cross-section changes depending on the direction of inclination, it is speculated that many columns incline around  $58^\circ$ . If these columns grew in [1 1 1] orientation, the apparent orientation of this crystal is detected as [1 1 0] in XRD measurement, because the (1 1 1) plane inclines at  $54.8^\circ$  to the (1 1 0) plane in an fcc crystal. To confirm this, pole figure elevation profile of crystalline orientation of micro-crystals in a single sample to the surface plane by the stereographic projection method [38]. The pole profile of sample A-1 shown in Fig. 7 reveals strong

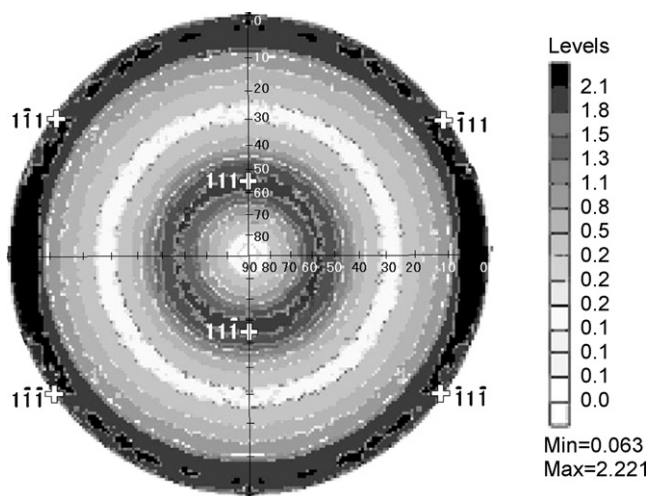


Fig. 7. (1 1 0) pole figure for sample A-1 indicating the tilt angle distribution of {1 1 1} micro-crystals to the surface plane. The symbol + corresponds to {1 1 1} of standard (1 1 0) projection of a cubic single crystal.

two peaks around  $0^\circ$  and  $55^\circ$  marked with +, corresponding to [1 1 1] of standard [1 1 0] projection of a cubic single crystal. This result indicates that the film contains micro-crystals of [1 1 1] orientation with tilting angle of ca.  $55^\circ$  to the substrate plane, and the tilting direction is randomly distributed.

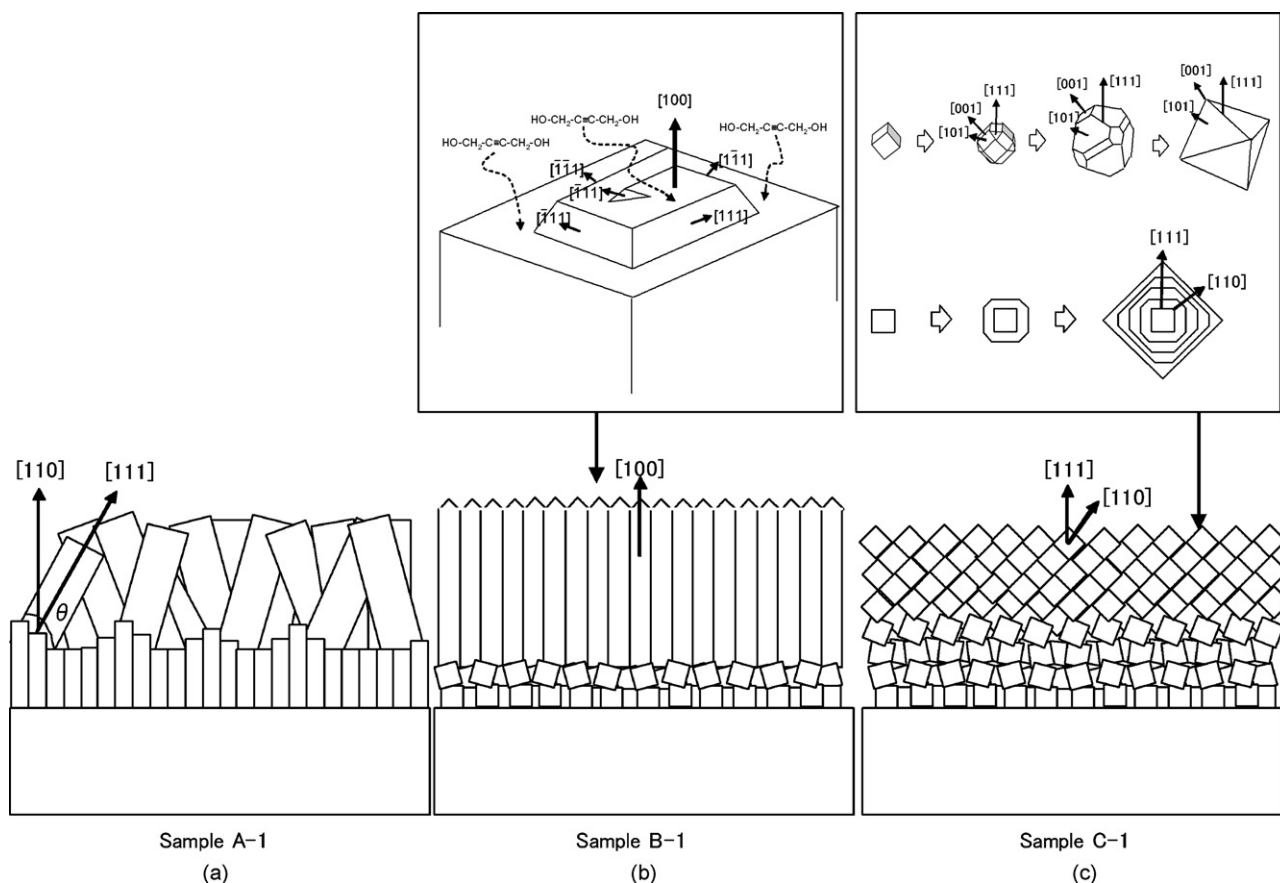
From the above discussion, Ni electrodeposits seem to grow in a manner predicted from the two-dimensional nuclei theory in which the growth plane is basically determined by crystallization overpotential related to supersaturation, but the growth axis is not always consistent with the preferred orientation axis. Models of electrodeposition of Ni films on Cu substrates are summarized in Fig. 8.

Fig. 8(a) shows a model for sample A-1. At the initial stage of electrodeposition, high density of nucleation causes growth of fine and dense columns in a direction normal to the substrate plane. Most of these columns are annihilated in competitive growth, and only a small number of thick columns survive and grow continuously at the (1 1 1) plane in the growing direction with tilting angle of ca.  $55^\circ$  to the substrate plane, resulting in apparent orientation of [1 1 0] observed in XRD measurement.

Fig. 8(b) is a model for sample B-1, in which columnar crystals grow on fine crystals. At the bottom of the film, a considerable amount of BD adsorbs on the surface, resulting in reduction of grain size due to an inhibitory effect on crystal growth. This effect is weakened but continues during the deposition process to keep the column thin. The top of each column continues to grow in a spiral manner shown in the top drawing in Fig. 8(b), i.e., orientation of the growing surface, [1 1 1], inclines to the mean growing direction, [1 0 0].

Fig. 8(c) is a model for sample C-1, and probably B-2 and C-2, in which the Ni film shows [1 1 1] orientation in XRD results as shown in Fig. 1, and the film is composed of lozenge-type crystals. The top drawing in Fig. 8(c) shows growth of lozenge-type crystals in which fast-growing plane tend to disappear and slow-growing plane tend to survive [39–41]. Such a manner of growth was observed for a KCl crystal with a high concentration of Pb impurity [41].

Structures and morphology of electrodeposits are affected by inhibition strength of BD related to its coverage on the surface and thus to its concentration in the bath. It is reasonable to speculate that the columnar crystal of sample B-1 was formed by continuous growth under the condition of weak inhibition, while fine crystals of sample C-1 were formed by intermittent growth under the condition of strong inhibition. The coverage of BD depends on orientation



**Fig. 8.** Schematic representation of electrodeposited Ni films on Cu substrates. (a) Sample A-1. BR-type crystals incline to fine columnar Ni crystals. (b) Sample B-1. FT-type columnar Ni crystals grow spirally on UD-type crystals. (c) Sample C-1. Fine lozenge UD-type crystals grow on the substrate.

of the surface. For example, coverage of the (1 1 1) plane seems to be smaller than that, for example, of the (1 0 0) plane because the deposition rate of Ni on the former is faster than that on the latter. Eventually, the (1 1 1) plane with faster deposition rate disappears as shown in the top drawing in Fig. 8(c), and, for example, the (1 1 0) plane with slower deposition rate becomes predominant on the deposited surface [39,42].

As discussed in this paper, the inhibitory effect of BD on the electroplating process is influenced by many factors such as overpotential and crystal orientation and provides variation of morphology and structures of plating films. It seems reasonable that BD molecule adsorbs on Ni surface mainly with its triple bond as on Pt [43] and Au [44]. Bron and Holtze proposed the adsorbed orientation model in which BD adsorbs on Au with strong interaction at the multiple bond and partial interaction at OH groups [44]. In the present case it is supposed that BD molecule adsorbs on Ni with co-deposition of Ni atoms and provides inhibitory effect. BD was co-deposited into the Ni deposits resulting in 0.220 wt% of carbon content in sample C-3 and 0.005 wt% in sample A-3 measured by total organic carbon analysis. Other adsorbents such as hydrogen [21–23] and Ni(OH)<sub>2</sub> [24] and anions such like SO<sub>4</sub><sup>2-</sup> or Cl<sup>-</sup> also have similar effects as shown in many previous studies. The cause and condition of spiral or slanting growth of crystals and their control remain as issues for future work.

#### 4. Conclusions

In this work, structure of Ni films electrodeposited from a Watts-type bath containing 2-buthyne-1,4-diol (BD) was investigated using SEM, cross-sectional SIM and XRD measurement with a pole

profiling technique and electrochemical methods. The relationship between structures and crystallographic orientation of electrodeposits and deposition condition was evaluated. The results obtained and conclusions based in the results are follows:

- (1) Preferred orientation of Ni electrodeposited films can be assigned to potential domains for electrodeposition. Preferred orientation in the potential region higher than  $-0.53$  V (SHE) (domain 1) was (1 1 0) or (1 0 0), that in the region from  $-0.54$  to  $-0.56$  V (domain 2) were (1 1 1) and (3 1 1), and that in the region lower than  $-0.59$  V (domain 3) was (1 0 0).
- (2) Preferred orientation observed by XRD measurement does not always agree with orientation of the actual growing plane because the growing plane may tilt to the geometric surface of the specimen. For example, preferred orientation of (1 1 0) observed in domain 1 can be assigned to growing (1 1 1) plane which tilts  $55^\circ$  to the substrate, and preferred orientation of (1 0 0) observed in domain 2 can be assigned to spiral growing (1 1 1) plane.
- (3) The growing axis of Ni electrodeposits in the lower overpotential region seems to agree with the speculation from Pangarov's model based on the two-dimensional nuclei theory in which the growth plane is fundamentally determined by crystallization overpotential related to supersaturation of adatoms, although the growth axes of Ni deposits do not always agree with the preferred orientation.
- (4) Adsorption of BD affects the structures and morphology of Ni electrodeposits via an inhibitory effect related to its surface coverage depending on deposition rate, surface orientation and BD concentration in the plating bath.

## Acknowledgements

The authors express their appreciation to Mr. Yoshiaki Yamada (Rigaku Corporation) and Mr. Hiroshi Chihara (TDK Corporation) for their contribution to pole figure analysis and their valuable discussion.

## References

- [1] J.W. Dini, *Electrodeposition: The Materials Science of Coatings and Substrates*, Noyes Publications, New Jersey, 1993, p. 163.
- [2] M. Paunovic, M. Schlesinger, *Fundamentals of Electrochemical Deposition*, John Wiley and Sons, New York, 1998, pp. 247, 253.
- [3] W. Dahms, R. Schmacher, J.M. McCaskie, *Plat. Surf. Finish.* 84 (5) (1997) 120.
- [4] L. Weininger, M.W. Breiter, *J. Electrochem. Soc.* 110 (1963) 484.
- [5] R. Hayanes, H.C. Ling, U.S. Patent 4,610,932 (1986).
- [6] T.F. Davis, D. Khan, U.S. Patent 4,934,968 (1990).
- [7] J.O'M. Bockris, A.K.N. Reddy, M. Gamboa-Aldeco, *Modern Electrochemistry 2A*, Plenum Press, New York, 2000, p. 978.
- [8] G.A. Di Bari, in: M. Schlesinger, M. Paunovic (Eds.), *Modern Electroplating*, 4th ed., John Wiley and Sons, New York, 2000, p. 149.
- [9] O.P. Watts, *Trans. Am. Electrochem. Soc.* 29 (1916) 395.
- [10] M. Schlöttor, U.S. Patent 1,972,693 (1934).
- [11] O. Kardos, T.J. Menzel, J.L. Sweet, U.S. Patent 2,712,522 (1955).
- [12] H. Brown, B.B. Knapp, in: F.A. Lowenheim (Ed.), *Modern Electroplating*, 3rd ed., John Wiley and Sons, New York, 1974, p. 287.
- [13] H. Fischer, *Elektrolytische Abcheidung und Elektrokristallisation von Metallen*, Springer-Verlag, Berlin, 1954, p. 422.
- [14] H. Fischer, *Electrodeposition Surface Treatment*, 1 (1972/73) 239.
- [15] H. Fischer, *Electrodeposition Surface Treatment*, 1 (1972/73) 319.
- [16] H. Fischer, *Angew. Chem. Int. Ed.* 8 (1969) 108.
- [17] H. Fischer, *Plating* 56 (1969) 1229.
- [18] R. Winand, *Hydrometallurgy* 29 (1992) 567.
- [19] R. Winand, *Electrochim. Acta* 39 (1994) 1091.
- [20] R. Winand, *J. Appl. Electrochem.* 21 (1991) 377.
- [21] A.K.N. Reddy, *J. Electroanal. Chem.* 6 (1963) 141.
- [22] A.K.N. Reddy, S.R. Rajagopalan, *J. Electroanal. Chem.* 6 (1963) 153.
- [23] A.K.N. Reddy, S.R. Rajagopalan, *J. Electroanal. Chem.* 6 (1963) 159.
- [24] J. Amblard, I. Epelboin, M. Froment, G. Maurin, *J. Appl. Electrochem.* 9 (1979) 233.
- [25] M. Motoyama, Y. Fukunaka, T. Sakka, Y.H. Ogata, *J. Electrochem. Soc.* 153 (2006) C502.
- [26] J. Macheras, D. Vouros, C. Kollia, N. Spyrellis, *Trans. I. M. F.* 74 (1996) 55.
- [27] T. Watanabe, *Nano Plating*, Elsevier Science, 2004, pp. 4, 29, 344.
- [28] N.A. Pangarov, *Electrochim. Acta* 7 (1962) 139.
- [29] N.A. Pangarov, *Electrochim. Acta* 9 (1964) 721.
- [30] N.A. Pangarov, *J. Electroanal. Chem.* 9 (1965) 70.
- [31] S. Haruyama, *Electrochemistry for Surface Finishing Engineers*, Maruzen, Tokyo, 2001, p. 110 (in Japanese).
- [32] J.O'M. Bockris, G.A. Razumney, *Fundamental Aspects of Electrocrystallization*, Plenum Press, New York, 1967, pp. 9, 81.
- [33] G.I. Finch, A.L. Williams, *Trans. Faraday. Soc.* 32 (1937) 564.
- [34] T. Seiyama, *Electrochemistry* 38 (1970) 707 (in Japanese).
- [35] T. Seiyama, *Electrochemistry* 42 (1974) 206 (in Japanese).
- [36] E.P. Pavlatou, M. Raptakis, N. Spyrellis, *Surface and Coating Technology* 201 (2007) 4571.
- [37] W.K. Burton, N. Cabrera, F.C. Frank, *J. Phil. Trans. Roy. Soc. London A: Math. Phys. Sci.* 243 (1951) 299.
- [38] H.P. Klug, L.E. Alexander, *X-ray Diffraction Procedures*, John Wiley & Sons, Inc., New York, 1974, p. 568.
- [39] J.O'M. Bockris, H. Kita, *J. Electrochem. Soc.* 109 (1962) 928.
- [40] J.O'M. Bockris, A.K.N. Reddy, M. Gamboa-Aldeco, *Modern Electrochemistry 2A*, Plenum Press, New York, 2000, p.1328.
- [41] L. Lian, K. Tsukamoto, I. Sunagawa, *J. Crystal Growth* 99 (1990) 1156.
- [42] I. Sunagawa, *Crystals: Growth, Morphology, and Perfection*, Cambridge University Press, Cambridge, 2005, p. 68.
- [43] J.Y. Gui, B.E. Kahn, C.-H. Lin, F. Lu, G.N. Salaita, D.A. Stem, D.C. Zapien, A.T. Hubbard, *J. Electroanal. Chem.* 252 (1988) 169.
- [44] M. Bron, R. Holtze, *Surf. Sci.* 457 (2000) 178.